Title
Shearing Behavior of Tire-Derived Aggregate with Large Particle Size. I: Internal and Concrete Interface Direct Shear

Journal
Journal of Geotechnical and Geoenvironmental Engineering, 143(10)

ISSN
1090-0241

Authors
Ghaaowd, Ismaail
McCartney, John S
Thielmann, Stuart S
et al.

Publication Date
2017-10-01

DOI
10.1061/(asce)gt.1943-5606.0001775

Peer reviewed

SHEARING BEHAVIOR OF TIRE DERIVED AGGREGATE WITH LARGE PARTICLE SIZE. I: INTERNAL AND CONCRETE INTERFACE DIRECT SHEAR

by Ismaail Ghaaowd, M.S., S.M. ASCE[1], John S. McCartney, Ph.D., P.E., M. ASCE[2], Stuart S. Thielmann, M.S., S.M. ASCE[3], Michael J. Sanders, M.S., S.M. ASCE[4] and Patrick J. Fox, Ph.D., P.E., F. ASCE[5]

ABSTRACT: Tire-Derived Aggregate (TDA) has been used widely in civil engineering applications such as highway embankments, light rail foundations, landslide repairs, and retaining walls as both a recycled material and a lightweight fill. Although the shearing properties of certain types of TDA have been studied, there is still a need for representative and reliable properties of TDA with large particles, such as Type B TDA with particle sizes ranging from 150 to 300 mm. Direct shear tests were performed on Type B TDA using a new large-scale shearing device to measure properties governing internal shear strength as well as interface shear strength against concrete. The internal failure envelope is nonlinear, with a secant friction angle decreasing from 39.6 to 30.2° as the normal stress increased from 19.5 to 76.7 kPa. Negligible shearing rate effects were observed for the internal shear strength of this material. The TDA-concrete interface failure envelope is linear with a friction angle of 22.6°. The dilation angle decreased with increasing normal stress for the TDA internal shear tests, whereas only contraction was observed for the TDA-concrete interface shear tests. Displacements at failure for the TDA internal shear tests ranged from 333 to 439 mm, and were 2 to 3 times larger than those for the TDA-concrete interface shear tests.

[1] Doctoral Candidate, Dept. of Structural Eng., Univ. of California San Diego, 9500 Gilman Dr., La Jolla, CA 92093-0085; ighaaowd@eng.ucsd.edu
[2] Associate Professor, Dept. of Structural Eng., Univ. of California San Diego, 9500 Gilman Dr., La Jolla, CA 92093-0085; mccartney@ucsd.edu
[3] Structural Engineer, Dept. of Structural Eng., Univ. of California San Diego, 9500 Gilman Dr., La Jolla, CA 92093-0085; mjsander@eng.ucsd.edu
[4] Staff Geotechnical Engineer, GeoEngineers, Inc., 1101 S Fawcett Ave # 200, Tacoma, WA 98402
[5] Shaw Professor and Head, Dept. of Civil and Environmental Engineering, The Pennsylvania State University, 212 Sackett Building, University Park, Pa 16802-1408; pjfox@engr.psu.edu

INTRODUCTION

Although waste tires are being generated at high rates in California (CalRecycle 2016a) as well as elsewhere in the U.S., research studies have found that they can be recycled in the form of Tire-Derived Aggregate (TDA) as a light-weight construction material (e.g., Ahmed and Lovell 1993; Geosyntec 2008; Ahn et al. 2014; CalRecycle 2016b). The unit weight of compacted TDA is approximately 5 to 9 kN/m^3, which is about one-third to one-half that of most granular backfill soils. Several projects have used tire shreds as a replacement for granular backfill in highway embankments or subgrades (Geisler et al. 1989; Ahmed and Lovell 1993; Bosscher et al. 1993; Bosscher et al. 1997; Hoppe 1998; Dickson et al. 2001; Tandon et al. 2007) and retaining walls (Humphrey et al. 1992, 1993; Tweedie et al. 1998; Xiao et al. 2012). These studies have found the performance of TDA fills to be comparable or better than soil-only fills. Despite the positive findings and recommendations of many full-scale studies, there are still uncertainties regarding the shearing properties of TDA. This is particularly true for TDA with large particles, such as Type B TDA material, which has not been adequately characterized due to limitations in the size and displacement capability of available shearing devices. To address this need, Fox et al. (2017) developed a novel large-scale combination direct shear/simple shear device for Type B TDA that can accommodate specimens measuring 3048 mm × 1220 mm in plan and up to 1830 m in height. This paper presents the results of TDA internal direct shear and TDA-concrete interface direct shear tests, which are the first to fully characterize the shear stress-displacement relationships and failure envelopes for Type B TDA. A companion paper (McCartney et al. 2017) presents corresponding cyclic simple shear data obtained using the same device in an alternate configuration.

BACKGROUND

TDA is composed of recycled waste tires that are shredded to a standard range of particle sizes. The two main categories of TDA used in practice are Type A TDA, with particle sizes ranging from 75 to 100 mm, and Type B TDA, with particle sizes ranging from 150 to 300 mm (ASTM D6270). Both types have limits on the amount of sidewall tire pieces and the quantity of particles having different lengths of exposed steel wire. However, Type B TDA requires less processing than TDA Type A, and is therefore more cost effective for earth fill applications. To minimize the likelihood for self-heating (Humphrey 1996; Arroyo 2011), fills constructed using Type B TDA are limited to having TDA layers up to 3 m thick, while those constructed from Type A TDA are limited to 1 m (ASTM D6270).

The shearing behavior of TDA, and in particular Type B TDA with large particles, is a topic that requires further attention. In the past, TDA shear strength has been typically determined using small direct shear boxes and standard soil testing procedures. A summary of the relevant studies that have reported shear stress-displacement relationships for TDA is presented in Table 1. In one of the earliest studies, Humphrey and Sandford (1993) and Humphrey et al. (1993) tested TDA having a maximum particle size of 76 mm in boxes with net dimensions of 286 × 286 mm and 387 × 387 mm in plan, both with a height of 228 mm. A clear peak shear strength value was not measured at the maximum displacement (35 mm) even though the box was approximately 4 times larger than the largest particle size. In a more recent study, Xiao et al. (2013) tested TDA having a maximum particle size of 75 mm in a larger box with dimensions of 790 × 800 mm in plan and 1219 mm in height, and clear peak shear strength values again were not clearly measured at the maximum displacement (160 mm), even though the box was 13 times larger than the largest particle size. Similar difficulties in measuring peak shear strengths from internal shear stress-displacement relationships were reported by Foose et al. (1996), Bernal et al. (1997), and Yang et al. (2002). Although one study (Gebhardt 1997) involved a large direct shear box (910 mm square) and observed clear peak shear strength values at a displacement of 230 mm, the TDA material was cut in the form of strips that did not meet the requirements of ASTM D6270. In many of these studies, direct shear tests were performed over a limited normal stress range, making it difficult to observe potential nonlinearity in the failure envelope. As a possible consequence, several studies have reported values of cohesion intercept for TDA internal shear strength (Humphrey and Sandford 1993; Xiao et al. 2013) and Strenk et al. (2007) found large variability of reported values of TDA friction angle in the literature, depending on the normal stress range of the tests.

As TDA has a high permeability, its shear strength is typically only characterized for drained conditions. As with soils, volume changes may occur during drained shearing of TDA, and it is relevant to characterize this behavior for the development of constitutive models. Yang et al. (2002) measured the internal shear strength of TDA in direct shear tests, and tracked the vertical change in height to infer shear-induced volume change behavior. They observed relatively large dilation for the specimens tested under low normal stresses. For larger normal stress, initial volumetric contraction was observed followed by a relatively large dilation.

Several studies have evaluated the internal shear strength of TDA with small particles (2-51 mm) using triaxial compression tests (Bressette 1984; Ahmed 1993; Benda 1995; Masad et al. 1996; Wu et al. 1997; Lee et al. 1999; Yang et al. 2002; Jeremić et al. 2004). Triaxial testing has the advantage that strains can be calculated, drainage can be controlled, and volume change can be evaluated for drained conditions. However, unless the specimen is very large (i.e., diameter > 1 m), the triaxial compression test would not allow sufficiently high axial strains to mobilize peak shear strength for Type B TDA.

The above studies on TDA internal shear strength indicate that a large direct shear device is required to test representative specimens of TDA and to reach values of shear displacement corresponding to failure (i.e., greater than 300 mm). Because large-scale testing devices generally have not been available, engineering designs using Type B TDA as backfill have been based on conservative estimates of shear strength, making it less competitive as an alternative fill material for civil engineering applications.

Fewer studies have measured the interface shear strengths between TDA and different geomaterials. In many applications, a nonwoven geotextile is placed between TDA and soil to act as a filter, while interfaces between concrete and TDA may be encountered with foundations and retaining walls (Humphrey et al. 1998). Gebhardt et al. (1997) investigated the interface between tire strips and glacial till for normal stresses ranging from 5.5 to 28 kPa. The interface friction angle decreased from 37° to 33° as the compaction water content of the glacial till was increased from 8% to 18-22% (dry to wet of optimum, respectively). This indicates that the characteristics of the interface material can affect interface shear strength with TDA. Bernal et al. (1997) found that the friction angle for a tire shred-woven polyester geotextile interface was 30°, and about 5° lower than the internal friction angle measured at 60 mm of shear displacement. Stark et al. (2010) investigated the interface shear strength between shredded tire pieces (size = 10 to 152 mm) and a nonwoven geotextile and a compacted silty clay. For relatively low normal stresses ranging from 4.8 to 19.2 kPa, the friction angles were 59° for the TDA-geotextile interface and 53° for the TDA-soil interface. Xiao et al. (2013) evaluated the interface shear strengths between Type A TDA and sand, concrete, nonwoven geotextile, and geogrid. They found that, different from TDA internal shear strength, shear stress-displacement relationships for these interfaces reached peak shear strength prior to the maximum displacement of the tests. For normal stresses ranging from 24 to

96 kPa, Xiao et al. (2013) measured interface friction angles of 39.3° for the TDA-sand interface, 35.5° for the TDA-concrete interface, 33.6° for the TDA-geotextile interface, and 18.8° for the TDA-geogrid interface. However, it is difficult to compare these values with the TDA internal friction angle of 36.1° because adhesion intercept values were also reported for the internal and interface tests. The source of adhesion is not apparent and likely indicates nonlinearity in the shear strength envelopes. Overall, the tests on TDA interfaces indicate that the interface friction angle may differ from the internal friction angle, albeit without clear trends.

Some studies have evaluated the performance of TDA mixed with soils (e.g., Edil and Bosscher 1994; Bosscher et al. 1997), and found that as the TDA percentage increased, the hydraulic conductivity and shear strength also increased. However, mixing TDA with soil requires additional construction effort and cost and may not provide a significant advantage over monolithic TDA fills from a mechanical or environmental sustainability perspective. Due to the minimal processing required, the most economical use of TDA is in monolithic fills with as large of particle size as permitted by regulations.

Several researchers have studied the effect of device size on shear strength test results. Humphrey and Sandford (1993) found that two large scale shear boxes (286 mm × 286 mm and 387 mm × 387 mm) gave nearly identical results for TDA. In-situ large direct shear devices (600 mm × 600 mm and 1200 mm × 1200 mm) were developed by Matsuoka et al. (2001) and used to test natural soils with different maximum particle sizes. They found that a ratio of the maximum particle size to box size of 4 was sufficient to produce consistent results. In addition, the effect of device size on the shear strength of sand having different densities was investigated by Cerato and Lutenegger (2006), who observed that the friction angle decreased as the area of the box increased due to less constraint on the formation of the failure plane. Wu et al. (2007) investigated the effect of specimen length to mean particle diameter ratio L/D_{50} on measured shear strength sand and sandy gravel using containers with L/D_{50} = 235 and L/D_{50} = 4700. The peak shear strength was observed decreasing with increasing L/D_{50} ratio.

MATERIALS

Information on particle size gradation for the Type B TDA material in the current study is presented in Table 2. Particles ranged in size from 30 to 320 mm, with a mean size D_{50} of 120 mm, and a thickness ranging from 6 to 20 mm. Typical particle shapes are shown in Figure 1. A few particles exceeded the maximum dimension limit of 300 mm, as defined by ASTM D6270. Due to the relatively flat and large size of the particles, these measurements required manual identification and sorting of particles by size as shown in Figure 1. As the particles have different shapes, their size was defined as the maximum dimension (i.e., length). A specific gravity of 1.15 was measured by weighing a porous plastic bag of TDA in air and submerged in water. This value is consistent with the corresponding value for crumb rubber (FHWA 1998) and the typical range of 1.02 to 1.27 for TDA (Bressette 1984; Humphrey et al. 1992; Humphrey and Manion 1992; Ahmed 1993).

EXPERIMENTAL EQUIPMENT AND PROCEDURES

Equipment

Schematic diagrams and a photograph of the large-scale combination direct shear/simple shear device developed by Fox et al. (2017) are shown in Figure 2, and a comparison of the characteristics of the device with those from other devices described in the literature is provided in Table 1. The device was designed to measure the internal shear strength of a full-height TDA specimen, as well as TDA-concrete interface shear strength by placing a large Portland cement concrete block into the bottom section of the box and shearing TDA material over the surface. The box has inside dimensions of 3048 × 1219 mm in plan and can accommodate specimens with a height up to 1830 mm plus the vertical distance of the shearing gap (typically 65 to 250 mm). As Type B TDA has particle sizes generally ranging from 150 to 300 mm, the minimum dimension of the device is 4 times larger than the maximum particle size. Although ASTM D3080 requires that the minimum specimen size be 10 times greater than the maximum particle size for direct shear tests, a factor of 4 was deemed suitable for Type B TDA because the particles are relatively flat in one dimension. Further, direct shear tests on soils with large particle sizes performed by Matsuoka et al. (2001) found that a factor of 4 was sufficient to obtain consistent shear strength results.

The large size of the box allows for a minimum shear displacement of 610 mm, which equals 20% of the inside length dimension. The sides of the box in the direction parallel to shear consist of stacked tubular steel members, while the sides of the box in the direction perpendicular to shear consist of vertical solid steel plates. In direct shear mode, the tubular members are restrained using four diagonal beams (i.e., one on each side of the upper and lower sections) so that the upper and lower rectangular sections remain rigid during shear and relative displacement occurs on a horizontal failure plane through the TDA. Two hydraulic actuators are used to provide the horizontal shearing force and are operated in displacement-control mode. Instrumentation includes a load cell on each actuator, four displacement transducers (i.e., one at each corner of the box) to measure vertical displacements, a string potentiometer to measure horizontal displacements, and tiltmeters to measure vertical end plate and actuator rotations. Additional details regarding design and evaluation of the device are provided by Fox et al. (2017) and the companion paper (McCartney et al. 2017).

Procedures

Before placement and compaction of the TDA material, the inside walls of the shear box were lined with 2 layers of plastic sheeting. The TDA was compacted in 100 mm-thick loose lifts using a self-propelled rolling and vibrating compactor having a weight of 14.4 kN and 6 passes per lift, resulting in an initial total unit weight of approximately 5.0 kN/m^3. The typical compaction process for TDA in the field involves a compactor with a weight of 90 kN and 6 passes per lift (ASTM D6270), but in that case the TDA is not constrained laterally. Manion and Humphrey (1992) found that the compaction energy had only a small effect (less than 5%) on the resulting unit weight of TDA for compaction efforts greater than 60% of the standard Proctor effort. The initial specimen thickness was measured after compaction. A rigid top plate was then placed on the TDA specimen to distribute the vertical load. An array of load cells connected to individual rigid plates used in preliminary tests indicated that the normal stress distribution was uniform using this approach.

Normal stress was applied to the TDA specimen by adding dead load weights directly to the top of the rigid top plate for tests with low normal stress (i.e., less than 40 kPa). For higher normal stress, these weights were applied using a rigid “saddle” frame (Fig. 1c) to lower the center of gravity and reduce the potential for tipping instability of the load. The normal stress values reported in this study are all representative of the vertical normal stress on the shearing plane, and include the weight of the TDA overlying the shearing plane and upper box. The change in specimen thickness was measured after the application of normal stress using transducers on the four corners of the box. The normal stress remained on the specimen for a minimum of 12 hours (overnight) before the start of shearing. This was found to be sufficient to accommodate initial creep deformations, such as those observed by Wartman et al. (2007), even though these creep displacements were negligible compared to the immediate settlement under the applied normal stress.

After the vertical loading process, four hydraulic jacks were used to raise the top section of the box to form a gap (65-250 mm) and avoid steel-on-steel contact during testing. This process is facilitated by the low friction of the plastic sheeting and by the fact that the normal load rests on the TDA specimen and not on the frame of the device. The gap is less than the maximum TDA particle size, even though most of the TDA particles were observed to be oriented with their flat direction perpendicular to the loading direction (i.e., horizontal). The rigid top plate was then connected to the top section frame so that the entire weight of the top half of the box, including the TDA specimen, frame and dead weights, constituted the vertical load applied to the shear plane. After the static loading period, the specimen was sheared in the air-dry condition and at constant displacement rate.

RESULTS

Internal Direct Shear

The testing program and results for eight internal direct shear tests on Type B TDA are summarized in Table 3. The first three tests, DS1 to DS3, were performed to investigate the effect of shear displacement rate, ranging from 1 to 100 mm/min, on the shear strength of Type B TDA at constant initial normal stress $\sigma_o \approx 24$ kPa. The remaining five tests, DS4 to DS8, were performed to characterize the failure envelope of Type B TDA over an initial normal stress range of 19.5 to 76.7 kPa and a displacement rate of 10 mm/min.

Tests DS1 to DS3 were performed first and included an extra compaction lift, resulting in greater unit weights before application of the initial normal stress than in tests DS4 to DS8. After application of the initial normal stress, the TDA specimens in Tests DS1-DS3 had total unit weights of approximately 6.5 kN/m^3, while the TDA specimens in Tests DS4-DS8 had total unit weights ranging from 6.01 to 8.04 kN/m^3 depending on the normal stress applied. After compaction, the specimens that were loaded to higher normal stresses experienced larger changes in volume, leading to a progressively denser condition. The TDA specimen unit weight was observed to increase immediately after the application of normal stress, followed by a small amount of creep settlement (less than 25 mm). The range of unit weights encountered after application of the initial normal stress are consistent with the general range of unit weights observed in many field applications (CalRecycle 2016b).

Values of total unit weight (i.e., dry unit weight due to the negligible water content) after normal stress application and prior to shear are shown in Figure 3(a) for tests DS4 to DS8. A consistent and slightly nonlinear increase in unit weight with initial normal stress is observed, with a maximum value of 8.04 kN/m^3 at σ_o = 76.7 kPa. The corresponding one-dimensional compression curve for this TDA material is shown in Figure 3(b). Compression of the individual TDA particles was neglected in the calculation of the void ratio because the normal stresses were relatively low and the particles have low volume compressibility as indicated by a Poisson's ratio of nearly 0.5 (Feng and Sutterer 2000). The compressibility is approximately log-linear and yields a compression index C_c = 0.8. Because the points on the compression curve represent final values (i.e., after application of normal stress) from different tests, a preconsolidation-type yield stress at low normal stress is not observed. Humphrey and Manion (1992) and Ahmed and Lovell (1993) found that particle gradation affects the compression curve of TDA, while Ahmed and Lovell (1993) noted that the slope of the compression curve for TDA may vary with compaction effort.

The shear stress-displacement relationships for tests DS1 to DS3 are shown in Figure 4(a), with values of shear stress corrected for changing failure surface area during displacement.

Despite the two orders of magnitude difference in displacement rates for these tests, the three relationships are nearly identical, especially up to the peak corrected shear stress value, and display similar values of initial stiffness, peak corrected shear stress, and displacement at peak. The mobilized secant friction angles, shown in Figure 4(b), are also similar, with a peak value occurring at a displacement of 332 to 366 mm. The peak secant friction angle coincides with the maximum principal stress ratio, a commonly used failure criterion for triaxial tests on granular materials (e.g., Lee and Seed 1967). Peak secant friction angles are used to estimate the factor of safety for limit equilibrium analyses; however, depending on serviceability requirements, failure may be defined for displacements smaller than those at the peak. The relationships in Figure 4(b) are not the same as those in Figure 4(a) because area corrections for both normal stress and shear stress offset when calculating the mobilized secant friction angle. In Figure 4(b), each test displays a post-peak reduction of approximately 10 to 20%. The corresponding volumetric strain relationships for tests DS1 to DS3 are shown in Figure 4(c), where negative values indicate expansion. For each test, the TDA specimens experienced initial compression followed by expansion, which is consistent with the direct shear behavior for medium dense granular soils.

The area-corrected shear stress-displacement relationships for tests DS4 to DS8 under different normal stresses are shown in Figure 5(a). Similar to natural soils, clear increases in both shear stiffness and peak corrected shear stress are observed with increasing normal stress. Although peak corrected shear stress values were observed for each test, the relationships for mobilized secant friction angle, shown in Figure 5(b), provide a better indication of failure conditions. Displacements at the maximum corrected shear stress [Fig. 5(a)] ranged from 370 to 587 mm, whereas displacements at the peak secant friction angle [Fig. 5(b)] ranged from 337 to 439 mm and occurred significantly before the maximum displacement of the direct shear box. The corresponding volumetric strains for tests DS4 to DS8 are shown in Figure 5(c), and again indicate expansion (dilation) after an initial contraction. In general, increasing levels of normal stress produce greater initial contraction and less dilation (expansion) thereafter, which is consistent with the shear-induced volume change behavior for natural granular soils (Lee and Seed 1967).

Concrete Interface Direct Shear

The testing program and results for the Type B TDA-concrete interface are summarized in Table 4. Four interface direct shear tests were performed to characterize the failure envelope. The range of initial normal stresses were similar to those evaluated for the TDA internal strength tests, but the initial unit weight after application of normal stress was slightly greater (≈ 6.0 kN/m^3). The total unit weights for all four tests after application of normal stress were relatively consistent with an average of 7.3 kN/m^3. The trend in total unit weight with normal stress is not as consistent as in the TDA internal tests, which may have occurred because the TDA was compacted to an initially higher total unit weight.

The area-corrected stress-displacement relationships for tests DSI1 to DSI4 are shown in Figure 6(a). These relationships show a clear yielding point at a displacement of 50 to 120 mm, but do not indicate peak corrected shear stress values due to the decreasing area and increasing normal stress during shear. On the other hand, the relationships for mobilized secant friction angle, shown in Figure 6(b), indicate clear peak values at displacements of approximately 130 to 255 mm. The displacements at the peak secant friction angle are significantly smaller than those measured in the TDA internal tests because the particles were observed to slide across the concrete surface in the TDA interface tests, whereas they were observed to twist around one another due to interlocking in the TDA internal tests. The results in Figure 6(b) indicate that the evolution of mobilized secant friction angle throughout each test is similar, with slightly higher values and earlier peak displacements for lower normal stress levels. The corresponding volumetric strain-displacement relationships for tests DSI1 to DSI4 shown in Figure 6(c) also display similar and nearly linear behavior with continuous contraction throughout the shearing process. The maximum volumetric strain values for the TDA-concrete interface shear tests are larger than for the TDA internal shear tests, which is attributed to the absence of interlocking-induced dilation for the interface tests.

ANALYSIS

Failure Evaluation

The TDA direct shear results indicate that area corrections have a significant effect on the values of shear stress and peak corrected shear stress values may not be reliable for defining the failure envelope or making comparisons among tests. However, the mobilized secant friction angles show a much clearer peak value for both the TDA internal and the TDA-concrete interface tests, and this was used as the failure criterion when evaluating stress-displacement relationships. Accordingly, the area-corrected normal stress and shear stress values at the displacement corresponding to the peak secant friction angle were defined as failure conditions, and are summarized in Table 2.

A plot of TDA internal shear strength as a function of shear displacement rate is shown in Figure 7. The shear strength values are nearly identical with small differences attributed to the different initial conditions. Accordingly, and also considering Fig. 3(b), it can be concluded shear displacement rate has a negligible effect on the shear strength of Type B TDA at low normal stress (e.g., at approximately 24 kPa).

The failure points for the five TDA internal shear strength tests performed at different normal stress levels and a rate of 10 mm/min are shown in Figure 8(a). Although the trend in Figure 8(a) appears approximately linear, a nonlinear relationship is indicated from the evaluation of the peak secant friction angles. Values of peak secant friction angle are shown in Figure 8(b) and follow a clear decreasing trend with increasing normal stress. Dry TDA particles are not expected to have inter-particle forces leading to cohesion, so this assumption together with the decreasing peak secant friction angle indicates that the failure envelope is nonlinear. This nonlinearity is further investigated using the shear strength model of Duncan et al. (1980):

$$\tau_f = \sigma_f tan(\phi_{sec}) \qquad (1)$$

where the secant friction angle variation with the normal stress at failure is:

$$\phi_{sec} = \Delta\phi log\left({}^{\sigma_f}/_{P_{atm}}\right) + \phi_0 \qquad (2)$$

where P_{atm} is atmospheric pressure (101.3 kPa) and $\Delta\phi$ and ϕ_0 are fitting parameters. The semi-logarithmic plot shown in Figure 8(c) indicates that this model provides a good fit to the internal shear strength data for Type B TDA. This analysis allows for direct interpretation of the nonlinear failure envelope and thus differs from approaches taken in previous studies on TDA shear strength.

Average dilation angles were calculated from the relationship:

$$\psi = sin^{-1}\left(\frac{\tan(\alpha)}{2+\tan(\alpha)}\right) \qquad (3)$$

where α is the slope of the change in height versus displacement curve, as follows:

$$\alpha = tan^{-1}\left(\frac{Maximum\ Contraction - Maximum\ Dilation}{Displacement\ at\ Maximum\ Contraction - Displacement\ at\ Maximum\ Dilation}\right) \qquad (4)$$

The average dilation angle for the TDA internal shear tests ranges from 1.2° to 3.1° as shown in Figure 8(b). The dilation angle is small compared with the secant friction angle, and displays a clear decreasing trend with increasing normal stress consistent with the behavior of granular soils (Lee and Seed 1967).

The failure points for the TDA-concrete interface are shown in Figure 9(a). Different from the internal TDA failure envelope, the TDA-concrete failure envelope is linear and has zero intercept. The corresponding secant friction angles, shown in Figure 9(b), display a slight decrease with increasing normal stress. In this case, the shear strength can be represented using the conventional equation for frictional soils:

$$\tau_f = \sigma_f tan(\phi) \quad (5)$$

where ϕ is constant. For the Type B TDA-concrete interface, an average secant friction angle ϕ_{sec} of 22.9° was calculated, and is close to the best-fit value of 22.6° to the data points shown in Figure 9(a). Only contraction was observed for the TDA-concrete interfaces, so the dilation angle can be assumed to be zero for the TDA-concrete interface.

Failure Envelope Comparison

A comparison of TDA internal and TDA-concrete interface failure envelopes is shown in Figure 10. Normal stresses at failure vary for these envelopes because the maximum mobilized secant friction angles are reached at different values of shear displacement. The failure envelopes indicated by Equations (1) and (5) are also shown and are in good agreement with the experimental data. The nonlinearity of the TDA internal failure envelope is more apparent when compared with the linear TDA-concrete interface failure envelope. Although TDA-concrete interface shear strength is nearly one-half that of TDA internal shear strength over the range of normal stresses evaluated, the TDA-concrete interface friction angle is higher than soil-concrete interface friction angles measured for silt (14°), silty sand or clayey sand (17°), and clean sand (17-22°), as reported in NAVFAC DM7 (NAVFAC 1986). Differences between the internal and interface failure envelopes are attributed to dilatancy and particle interlocking for the TDA internal tests versus sliding of particles over the rough surface in the TDA-concrete interface tests. A comparison of the TDA internal shear stresses at failure with data reported from other studies in the literature is shown in Figure 11. Shear stress values at failure from the current study are in close agreement and lie toward the upper bound of other published values.

Initial Stiffness

Values of TDA initial shear stiffness, as obtained from the hyperbolic model of Duncan et al. (1980), are presented in Figure 12. The corrected shear stress-displacement relationships were normalized by dividing the shear displacement by the corrected shear stress, and then plotting versus the shear displacement. The inverse of the slope of this normalized corrected shear stress-displacement relationship corresponds to the initial stiffness of the corrected shear stress-displacement relationship. In each case, the fitting process was based on the corrected shear stress-displacement data preceding the peak secant friction angle. Shear stiffness increases with increasing normal stress for both the TDA internal and TDA-concrete interface tests, with significantly higher values for the TDA-concrete interface. Initial shear stiffness is larger for the TDA-concrete interface tests because failure occurred at smaller displacements.

CONCLUSIONS

This study investigated shear stress-displacement relationships and failure envelopes for large-size (Type B) tire derived aggregate (TDA). Large-scale direct shear tests were performed to measure the properties governing TDA internal shear strength as well as interface shear strength with Portland cement concrete. The internal failure envelope was nonlinear, with a peak secant friction angle that decreases from 39.6° at low normal stresses (19.5 kPa) to 30.2° at high normal stresses (76.7 kPa). The unit weight of TDA in these tests ranged from 6.01 to 8.04 kN/m^3, which is about 25 to 50% of the unit weight of typical natural backfill soils. Negligible displacement rate effects were observed for TDA internal shear strength.

The TDA-concrete interface failure envelope was linear, with a friction angle of 22.6°. The TDA-concrete interface friction angle is higher than typical values for interfaces between concrete and silt, clayey sand, or clean sand. Similar to granular soils, the dilation angle decreased with increasing normal stress for the internal TDA direct shear tests. Only contraction was observed during the TDA-concrete interface direct shear tests. The initial shear stiffness from the TDA-concrete interface shear tests was greater than from the TDA internal shear tests. These higher shear stiffness values correspond to a displacement at failure of approximately 130 to 255 mm for the TDA-concrete interface shear tests as opposed to a displacement at failure of 332 to 439 mm for the TDA internal shear tests.

ACKNOWLEDGMENTS

Financial support from California Department of Resources Recycling and Recovery (CalRecycle) for project DRR11064, and in particular the assistance of Stacey Patenaude and Bob Fujii of CalRecycle and Joaquin Wright of GHD Consultants, Sacramento, is gratefully acknowledged. The authors also thank the staff of the Powell Laboratories at UCSD for assistance with the experimental work. The contents of this paper reflect the views of the authors and do not necessarily reflect the views of the sponsor.

APPENDIX I. REFERENCES

Ahmed, I. (1993). Laboratory Study on Properties of Rubber Soils. Report No. FHWA/IN/JHRP-93/4, Purdue University, West Lafayette, Indiana.

Ahmed, I. and Lovell, C.W. (1993). "Rubber soils as lightweight geomaterials." Transportation Research Record. 1422, 61-70.

Ahn, I., Cheng, L., Fox, P.J., Wright, J., Patenaude, S., and Fujii, B. (2014). "Material properties of large-size tire derived aggregate for civil engineering applications." Journal of Materials in Civil Engineering, DOI: 10.1061/(ASCE)MT.1943-5533.0001225, 04014258.

American Society for Testing and Materials. (2011). ASTM D3080: Standard Test Method for Direct Shear Test of Soils under Consolidated Drained Conditions. ASTM International, West Conshohocken, PA.

American Society for Testing and Materials. (2012). ASTM D6270: Standard Practice for Use of Scrap Tires in Civil Engineering Applications. ASTM International, West Conshohocken, PA.

Arroyo, M., San Martin, I., Olivella, S. and Saaltink, M.W. (2011). "Evaluation of self-combustion risk in tire-derived aggregate fills." Waste Management. 31(9-10), 2133-2141.

Bernal, A., Salgado, R., Swan Jr., R.H. and Lovell, C.W. (1997). "Interaction between tire shreds, rubber-sand and geosynthetics." Geosynthetics International. 4(6), 623-643.

Bosscher, P.J., Edil, T.B., and Eldin, N. (1993). "Construction and performance of shredded waste tire test embankment." Transportation Research Record. Transportation Research Board, Washington, DC. Volume 1345, 44-52.

Bosscher, P.J., Edil, T.B., and Kuraoka, S. (1997). "Design of highway embankments using tire chips." Journal of Geotechnical and Geoenvironmental Engineering. 123(4), 295-304.

Bressette, T. (1984). Used Tire Material as an Alternate Permeable Aggregate. State of California, Department of Transportation, Division of Engineering Services, Office of Transportation Laboratory, Sacramento, CA.

CalRecycle. (2016a). California Waste Tire Market Report: 2015. Publication # DRRR 2016-01567. Sacramento, CA.

CalRecycle. (2016b). Usage Guide: Tire-Derived Aggregate (TDA). Publication # DRRR 2016-01545. Sacramento, CA.

Cerato, A.B. and Lutenegger, A.J. (2006). "Specimen size and scale effects of direct shear box tests of sands." Geotechnical Testing Journal, 31(1), 507-516.

Dickson, T.H., Dwyer, D.F., Humphrey, D.N. (2001). "Prototype tire-shred embankment construction." Transportation Research Record, 1755, National Research Council, Transportation Research Board, Washington, D.C. pp. 160-167.

Duncan, J.M., Byrne, P., Wong, K.S. and Mabry, P. (1980). Strength, Stress-strain and Bulk Modulus Parameters for Finite Element Analysis of Stresses and Movements in Soil Masses. Report No. UCB/GT/80-01, Dept. Civil Engineering, U.C. Berkeley.

Edil, T.B. and Bosscher, P.J. (1994). "Engineering properties of tire chips and soil mixtures." Geotechnical Testing Journal, 17(4), 453-464.

Federal Highway Administration, U.S. Department of Transportation. (1998). User Guidelines for Waste and Byproduct Materials in Pavement Construction. Publication Number: FHWA-RD-97-148.

Feng, Z.Y. and Sutterer, K.G. (2000). "Dynamic properties of granulated rubber/sand mixtures." ASTM Geotechnical Testing Journal. 23(3), 338–344.

Foose, G.J., Benson, C.H., and Bosscher, P.J. (1996). "Sand reinforced with shredded waste tires." Journal of Geotechnical Engineering. 122(9), 760-767.

Fox, P.J., Sanders, M., Latham, C., Ghaaowd, I., and McCartney, J.S. (2017). "Large-scale direct-simple shear test for large-particle tire-derived aggregates." ASTM Geotechnical Testing Journal. Accepted.

Gebhardt, M.A. (1997). Shear Strength of Shredded Tires as Applied to the Design and Construction of a Shredded Tire Stream Crossing, MS Thesis, Iowa State University.

Geisler, E., Cody, W.K., and Niemi, M.K. (1989). “Tires for subgrade support.” Annual Conference on Forest Engineering, Coeur D’Alene, ID. 1-5.

Geosyntec. (2008). Guidance Manual for Engineering Uses of Scrap Tires. Prepared for Maryland Department of the Environment. Geosyntec Project No.: ME0012-11.

Hoppe, E.J. (1998). “Field study of shredded-tire embankment,” Transportation Research Record No. 1619, Transportation Research Board, Washington, DC. 47-54.

Humphrey, D.N. (1996). Investigation of Exothermic Reaction in Tire Shred Fill Located on SR100 in Ilwaco, Washington. Report to Federal Highway Administration, Washington, DC.

Humphrey, D.N., Whetten, N., Weaver, J., Recker, K., Cosgrove, T.A. (1998). “Tire shreds as lightweight fill for embankments and retaining walls.” ASCE Geotechnical Special Publication No. 79, ASCE, Reston, Virginia. 1-15.

Humphrey, D.N., Sandford, T.C., Cribbs, M.M., Gharegrat, H., and Manion, W.P. (1992). Tire Chips as Lightweight Backfill for Retaining Walls - Phase I. Report to the New England Consortium, 137 pp.

Humphrey, D.N. and Manion, W.P. (1992). “Properties of tire chips for lightweight fill.” Grouting, Soil Improvement and Geosynthetics, R.H. Borden, et al., eds., ASCE, Vol. 2, 1344-1355.

Humprey, D.N. and Sandford, T.C. (1993). “Tire chips as lightweight subgrade fill and retaining wall backfill.” Symposium on Recovery and Effective Reuse of Discarded Materials and By-products for Construction of Highway Facilities. Denver, Colorado. 1-20.

Humphrey, D., Sandford, T., Cribbs, M., and Manion, W. (1993). "Shear strength and compressibility of tire chips for use as retaining wall backfill." Transportation Research Record. Transportation Research Board, Washington, DC. 1422, 29–35.

Jeremić, B., Putnam, J., Sett, K., Humphrey, D., Patenaude, S. (2004). "Calibration of elastic–plastic material model for tire shreds." GeoTrans 2004. ASCE. 760-767.

NAVFAC (1986). Soil Mechanics Design Manual 7 (DM7).

Lee, K.L., and Seed, H.B. (1967). "Drained strength characteristics of sands." Journal of the Soil Mechanics and Foundation Division. SM6, 118-143.

Lee, J.H., Salgado, R., Bernal, A., and Lovell, C.W. (1999). "Shredded tires and rubber-sand as lightweight backfill." Journal of Geotechnical and Geoenvironmental Engineering. 125(2), 132–141.

Manion, W.P. and Humphrey, D.N. (1992). "Use of tire shreds as lightweight and conventional embankment fill, Phase I – laboratory." Technical Paper 9I-I, Technical Services Division, Maine Department of Transportation, Augusta, ME.

Matsuoka, H., Liu, S., Sun, D., and Nishikata, U. (2001). "Development of a new in-situ direct shear test." Geotechnical Testing Journal. 24(1), 92–102.

McCartney, J. S., Ghaaowd, I.,, Fox, P. J., Sanders, M. J., Thielmann, S. S., and Sander, A. C. (2017). "Shearing behavior of tire derived aggregate with large particle size. I. Cyclic simple shear." Journal of Geotechnical and Geoenvironmental Engineering. Companion paper.

Stark, T.D., Reddy, K.R. and Marella, A. (2010). "Beneficial use of shredded tires as drainage material in cover systems for abandoned landfills." Journal of Hazardous, Toxic, and Radioactive Waste Management. 14(1), 47-60.

Strenk, P.M., Wartman, J., Grubb, D.G., Humphrey, D.N., and Natale, M.F. (2007). “Variability and scale-dependency of tire-derived aggregate.” Journal of Materials in Civil Engineering. 19(3), 233–241.

Tandon, V., Velazco, D.A., Nazarian, S., and Picornell, M. (2007). “Performance monitoring of embankments containing tire chips: Case study.” Journal of Performance of Constructed Facilities. 21(3), 207–214.

Tweedie, J.J., Humphrey, D.N., and Sandford, T.C. (1998). “Tire shreds as retaining wall backfill, active conditions.” Journal of Geotechnical and Geoenvironmental Engineering. 124(11), 1061-1070.

Xiao, M., Ledezma, M., and Hartman, C. (2013). “Shear resistance of tire-derived aggregate using large-scale direct shear tests. Journal of Materials in Civil Engineering. 04014110-1-8.

Xiao, M., Bowen, J., Graham, M., and Larralde, J. (2012). “Comparison of seismic responses of geosynthetically-reinforced walls with tire-derived aggregates and granular backfills.” Journal of Materials in Civil Engineering. 24(11), 1368-1377.

Wartman, J., Natale, M.F., and Strenk, P.M. (2007). “Immediate and time-dependent compression of tire-derived aggregate.” Journal of Geotechnical and Geoenvironmental Engineering. 33(3), 245-256.

Wu, W.Y., Benda, C.C. and Cauley, R.F. (1997). “Triaxial determination of shear strength of tire chips.” Journal of Geotechnical and Geoenvironmental Engineering. 123(5), 479-482.

Wu, P.K., Matsushima, K., and Tatsuoka, F. (2007). “Effects of specimen size and some other factors on the strength and deformation of granular soil in direct shear tests.” Geotechnical Testing Journal. 31(1), 1- 20.

Yang, S., Lohnes, R.A., and Kjartanson, B.H. (2002). “Mechanical properties of shredded tires.” Geotechnical Testing Journal. 25(1), 44-52.

Table 1: Summary of direct shear testing programs for TDA internal shear strength.

Test Parameters and Results	**Humphrey and Sandford (1993) and Humprey et al. (1993)**	**Foose et al. (1996)**	**Bernal et al. (1997)**	**Gebhardt (1997)**	**Yang et al. (2002)**	**Xiao et al. (2013)**	**This Study**
Box shape	Square	Circular	Square	Square	NR	Rect.	Rect.
Shear box areal dimensions (mm)	286×286 and 387×387	279 (dia)	300× 300	910× 910	NR	790× 800	3048× 1219
Shear box height (mm)	228	314	225	810	NR	1219	1830
Box width to maximum particle size ratio	3.8-5.0	2.1	6	2.1	NR	10.5	4
Maximum shear box displacement (mm)	35	90	60	230	25	180	690
Shearing rate (mm/min)	7.6	1.3	1	1	1	22	1-100
Maximum TDA size (mm)	76	150	50	432	10	75	320
Average unit weight (kN/m^3)	5.5	5.9	5.9	5.6	5.73	7.91-13.2	5.04-8.04
Normal stress range (kPa)	17-68	9-50	7-54	5.5-28		24-96	19.5-76.7
Maximum normal stress (kPa)	68	80	54	28	83	96	88.4
Internal friction angle (degrees)	19-26	30	35*	38	32	36.1	30.2-41.1
Apparent cohesion (kPa)	4.3-11.5	3	0	0	0	14.3	0

*Reported at the end of shearing

Table 2: Particle size information for Type B TDA material.

Parameter	Value
Range of particle size	30-320 mm
Range of particle thickness	6-20 mm
D_{10}*	70 mm
D_{30}*	105 mm
D_{50}*	120 mm
D_{60}*	155 mm
Coefficient of curvature, C_z	1.02
Coefficient of uniformity, C_u	2.21

*D_{10}, D_{30}, D_{50}, and D_{60} are the largest TDA particle dimensions at 10%, 30%, 50%, and 60% finer by dry weight.

Table 3: Summary of Type B TDA internal direct shear testing program and results.

Test	Initial* Normal Stress, σ_o (kPa)	Initial* Total Unit Weight (kN/m^3)	Initial* Void Ratio	Displacement Rate (mm/min)	Values At Peak Secant Friction Angle				Average Dilation Angle, ψ (deg)
					Normal Stress, σ_f (kPa)	Shear Strength, τ_f (kPa)	Secant Friction Angle, ϕ_{sec} (deg)	Displacement, δ_f (mm)	
DS1	23.8	6.45	0.75	1	27.0	23.5	41.0	366	3.6
DS2	23.8	6.60	0.71	10	26.7	23.1	40.8	337	4.7
DS3	24.3	6.56	0.72	100	27.3	22.9	40.0	332	3.7
DS4	19.5	6.01	0.87	10	21.9	17.7	38.8	337	2.9
DS5	22.9	6.11	0.85	10	25.8	21.3	39.6	344	3.1
DS6	38.8	6.95	0.62	10	44.6	31.4	35.1	400	2.6
DS7	60.8	7.58	0.49	10	71.0	46.5	33.3	439	1.3
DS8	76.7	8.04	0.40	10	88.3	51.5	30.2	403	1.2

*Initial values are at the start of shearing

Table 4: Summary of Type B TDA-concrete interface direct shear testing program and results.

Test	Initial* Normal Stress, σ_o (kPa)	Initial* Unit Weight (kN/m^3)	Initial* Void Ratio	Displacement Rate (mm/min)	Values At Peak Secant Friction Angle			
					Normal Stress, σ_f (kPa)	Shear Strength, τ_f (kPa)	Secant Friction Angle, ϕ_{sec} (deg)	Displacement, δ_f (mm)
DSI1	22.3	7.26	0.55	10	23.3	10.2	23.7	130
DSI2	39.5	7.12	0.58	10	42.0	17.5	22.6	185
DSI3	55.4	7.40	0.52	10	58.2	24.9	23.1	148
DSI4	77.0	7.38	0.53	10	83.9	34.4	22.3	255

*Initial values are at the start of shearing

LIST OF FIGURES

Figure 1

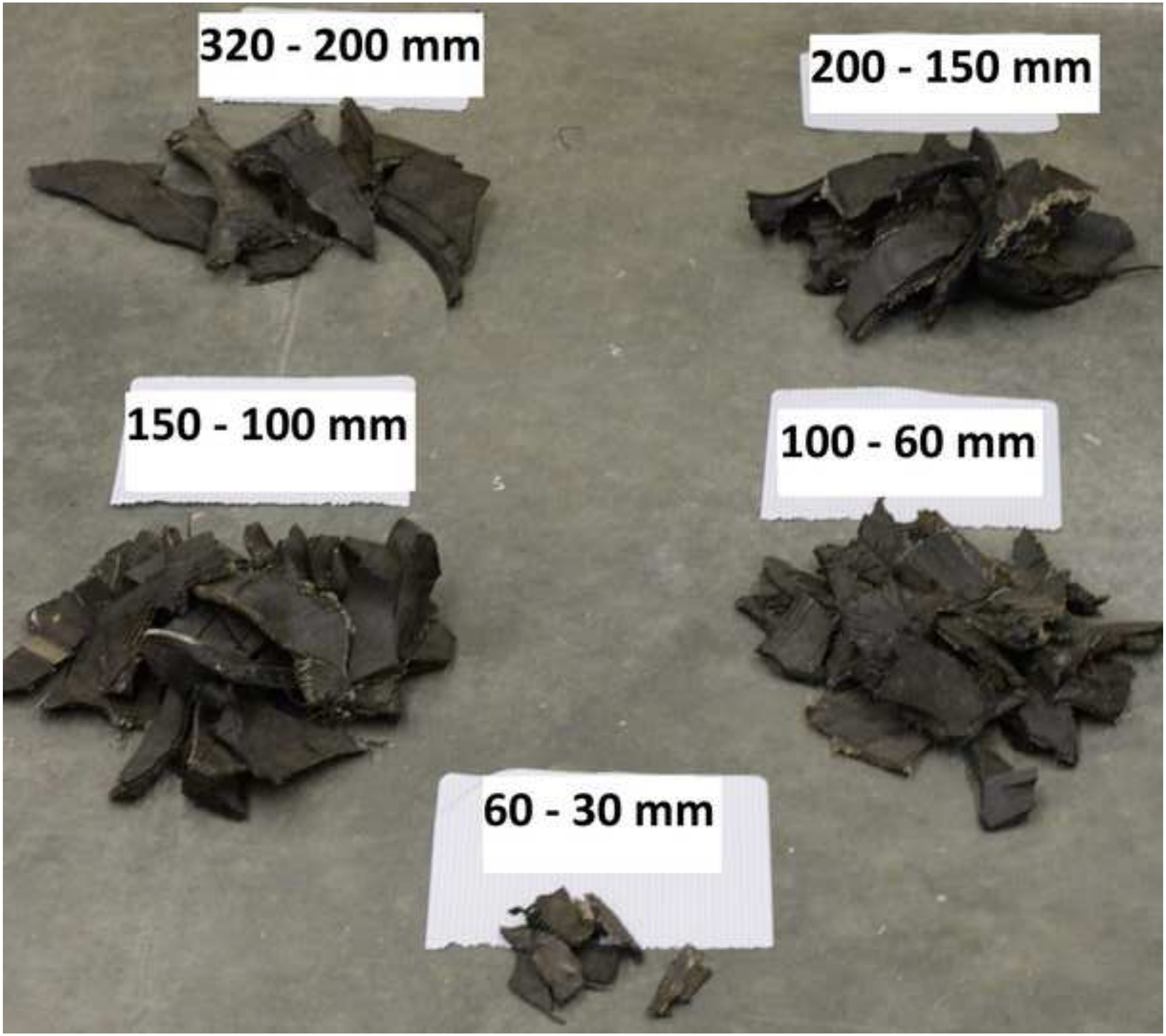

Figure 2 Click here to download Figure Figure 02.tif

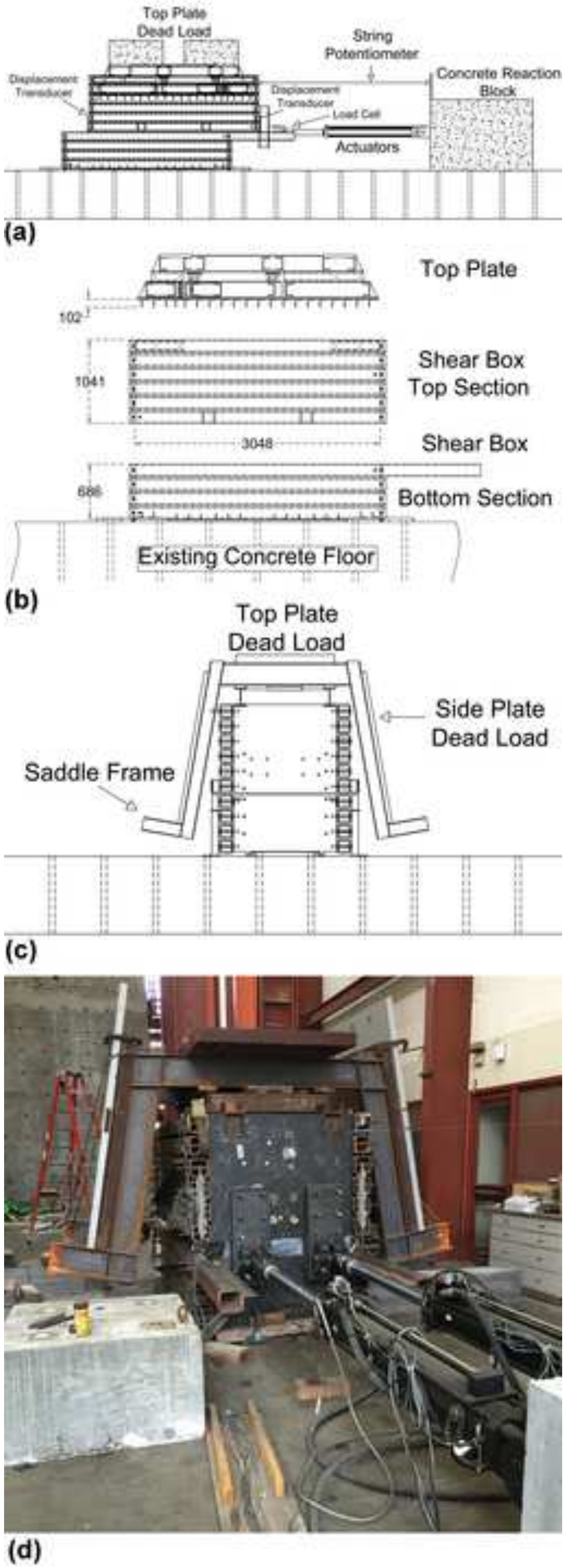

Figure 3

Click here to download Figure Figure 03.tif

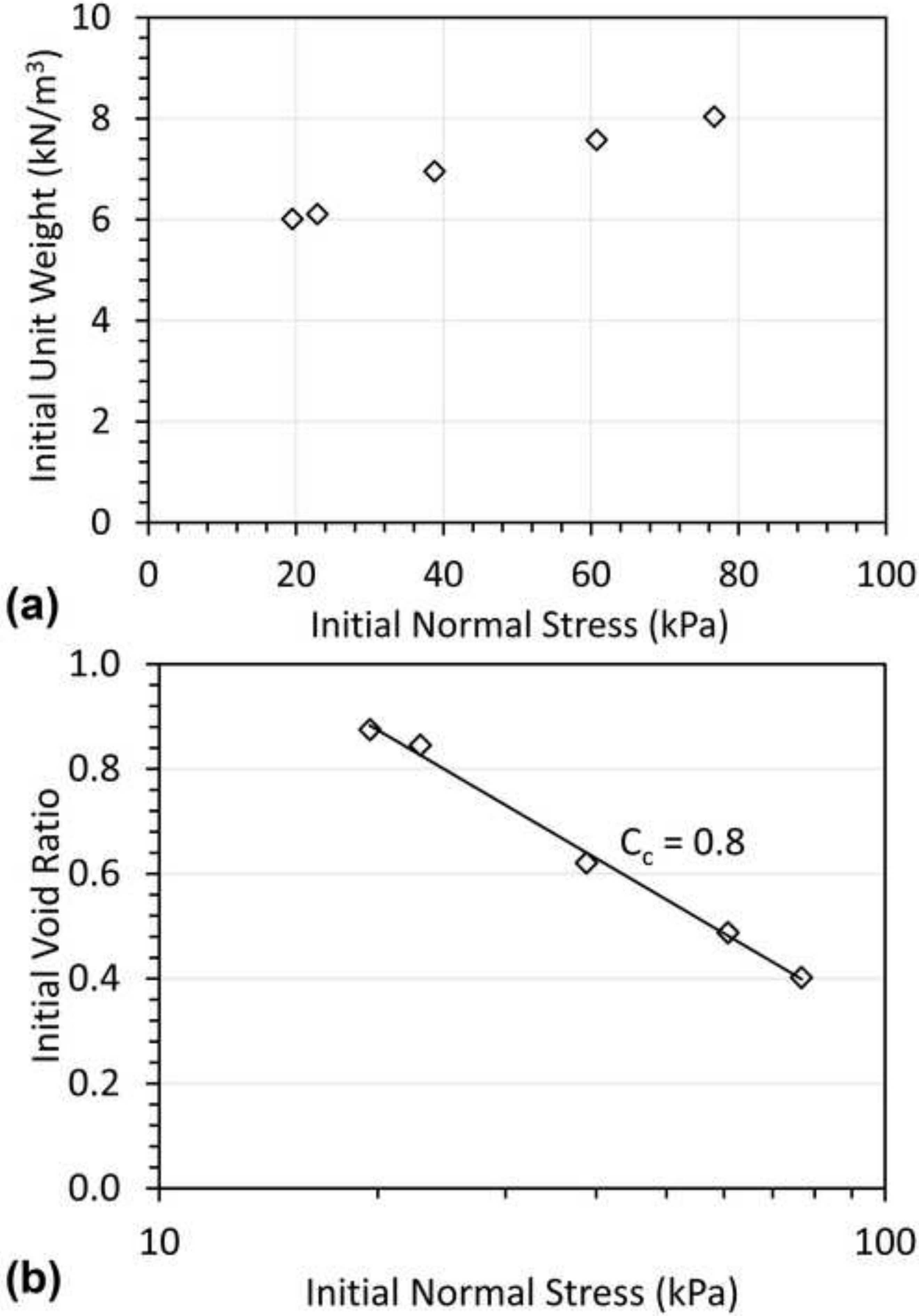

Figure 4

Click here to download Figure Figure 04.tif

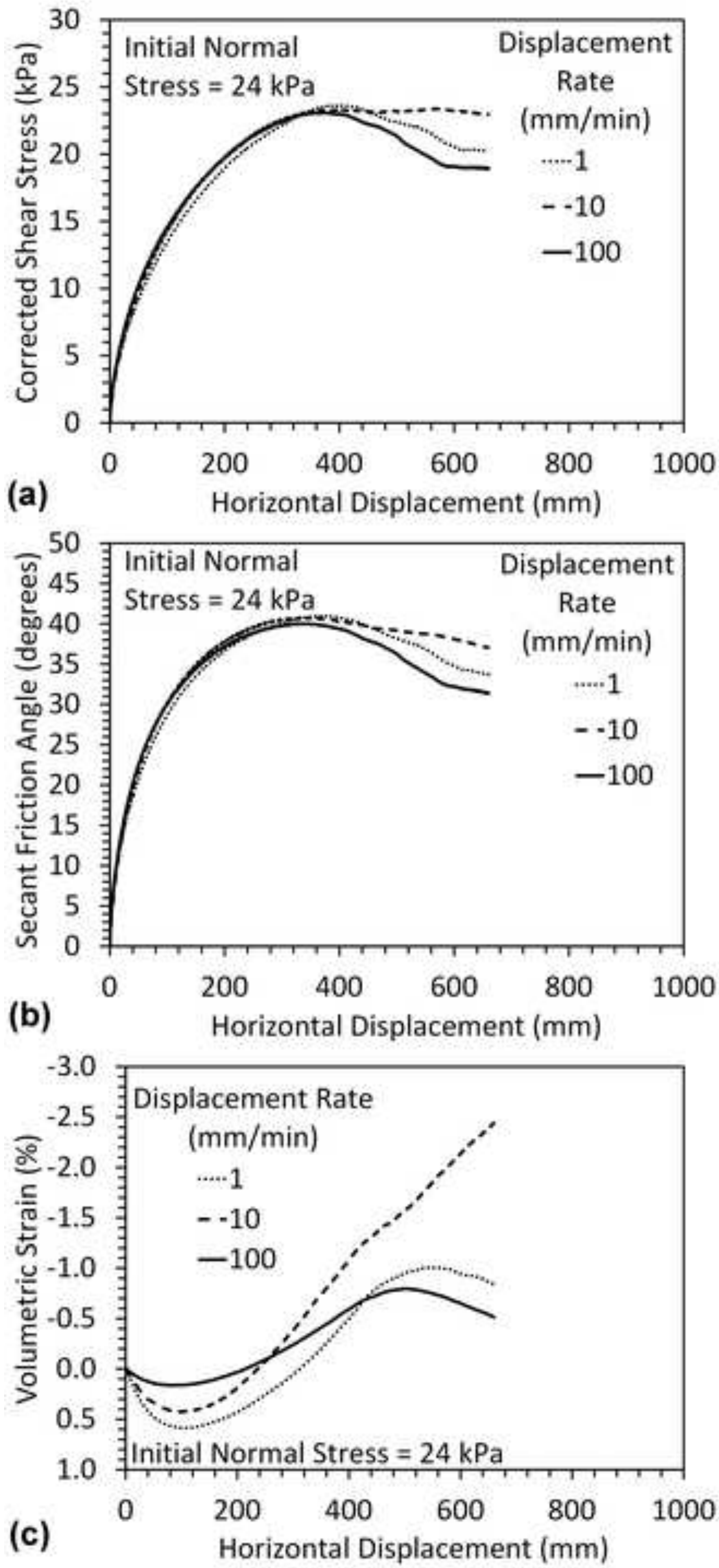

Figure 5

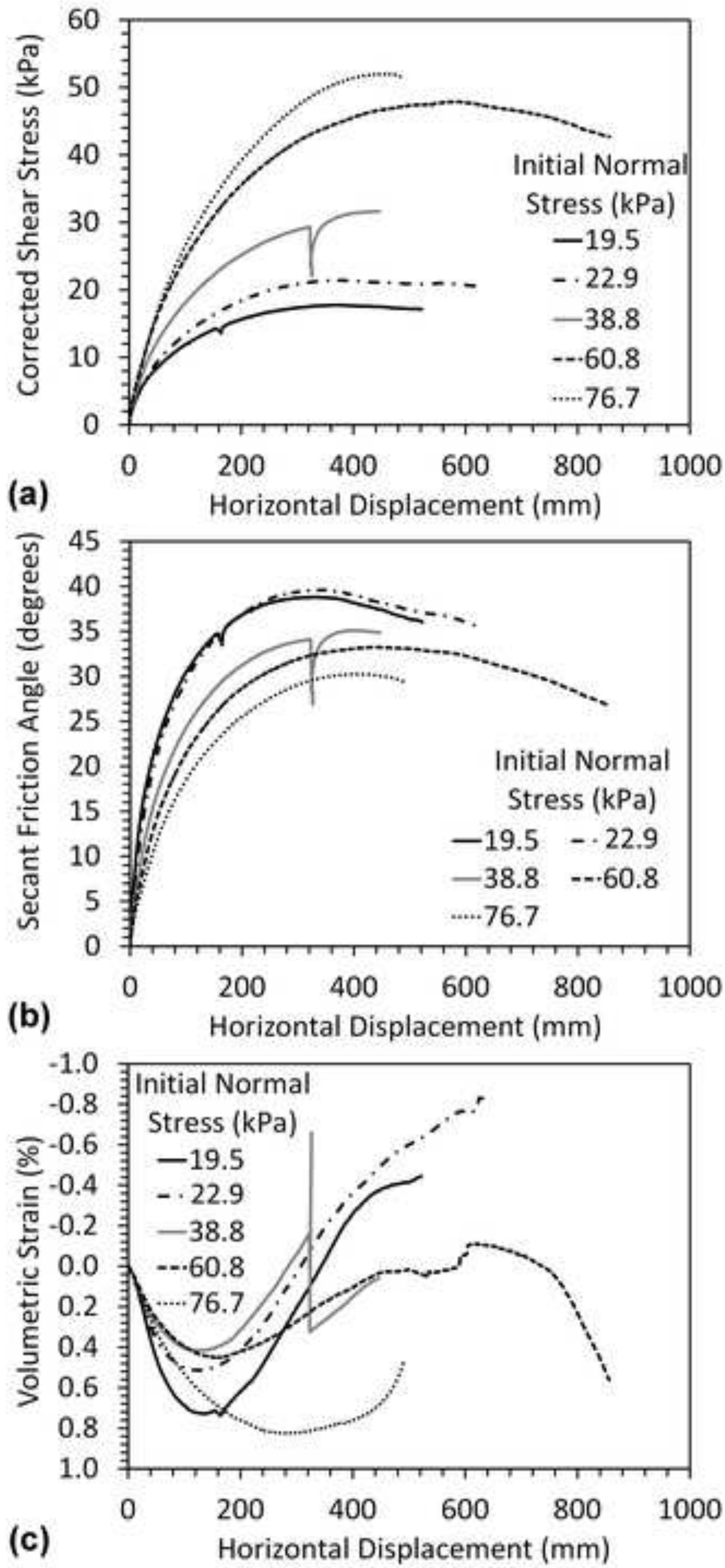

60
50
40
30
20
10
0
Corrected Shear Stress (kPa)
Initial Normal
Stress (kPa)
19.5
22.9
38.8
60.8
76.7
0
200
400
600
800
1000
(a)
Horizontal Displacement (mm)
45
40
35
30
25
20
15
10
5
0
Secant Friction Angle (degrees)
Initial Normal
Stress (kPa)
19.5
22.9
38.8
60.8
76.7
0
200
400
600
800
1000
(b)
Horizontal Displacement (mm)
-1.0
-0.8
-0.6
-0.4
-0.2
0.0
0.2
0.4
0.6
0.8
1.0
Volumetric Strain (%)
Initial Normal
Stress (kPa)
19.5
22.9
38.8
60.8
76.7
0
200
400
600
800
1000
(c)
Horizontal Displacement (mm)

Figure 6

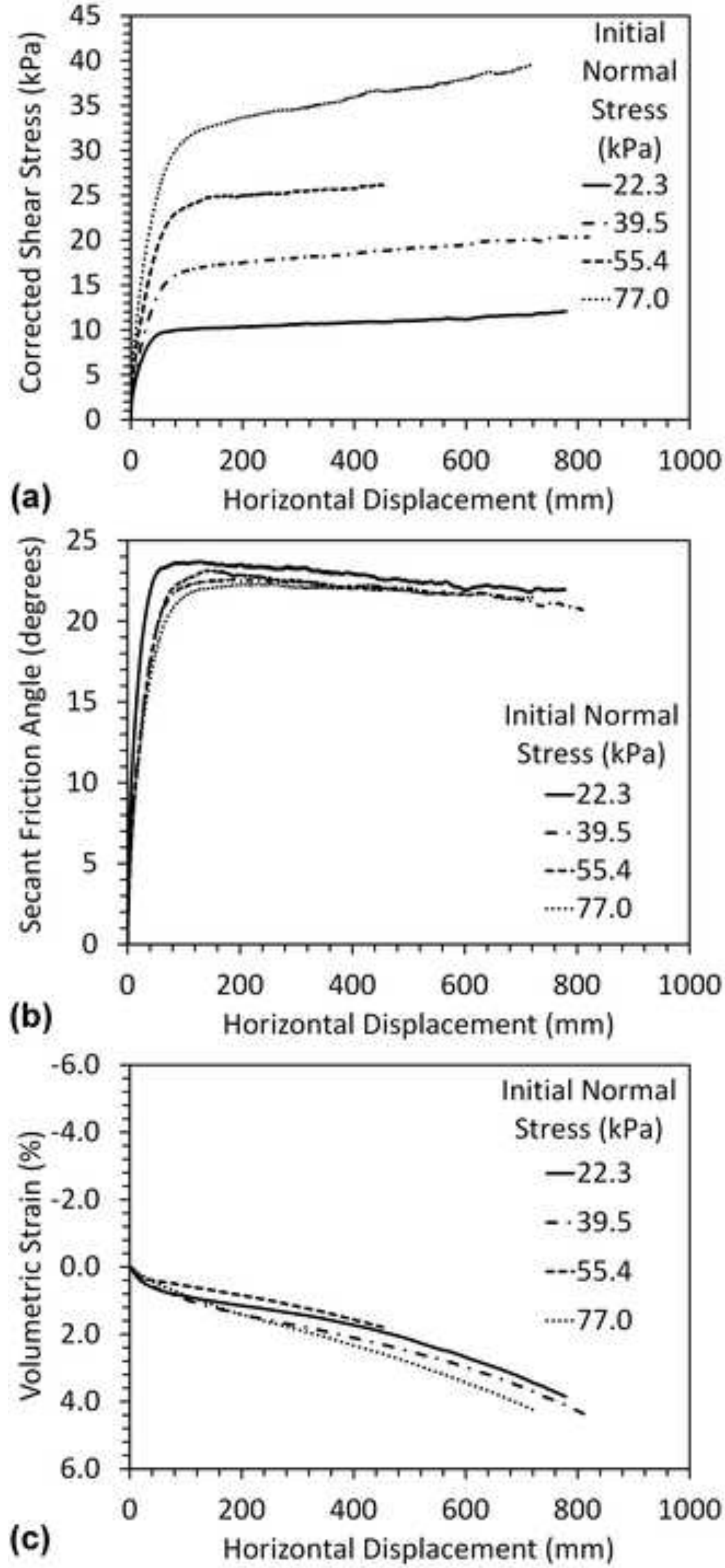

Corrected Shear Stress (kPa)
45
40
35
30
25
20
15
10
5
0
0
200
400
600
800
1000
Horizontal Displacement (mm)
Initial Normal Stress (kPa)
—22.3
- · 39.5
---55.4
·····77.0
(a)
Secant Friction Angle (degrees)
25
20
15
10
5
0
0
200
400
600
800
1000
Horizontal Displacement (mm)
Initial Normal Stress (kPa)
—22.3
- · 39.5
---55.4
·····77.0
(b)
Volumetric Strain (%)
-6.0
-4.0
-2.0
0.0
2.0
4.0
6.0
0
200
400
600
800
1000
Horizontal Displacement (mm)
Initial Normal Stress (kPa)
—22.3
- · 39.5
---55.4
·····77.0
(c)

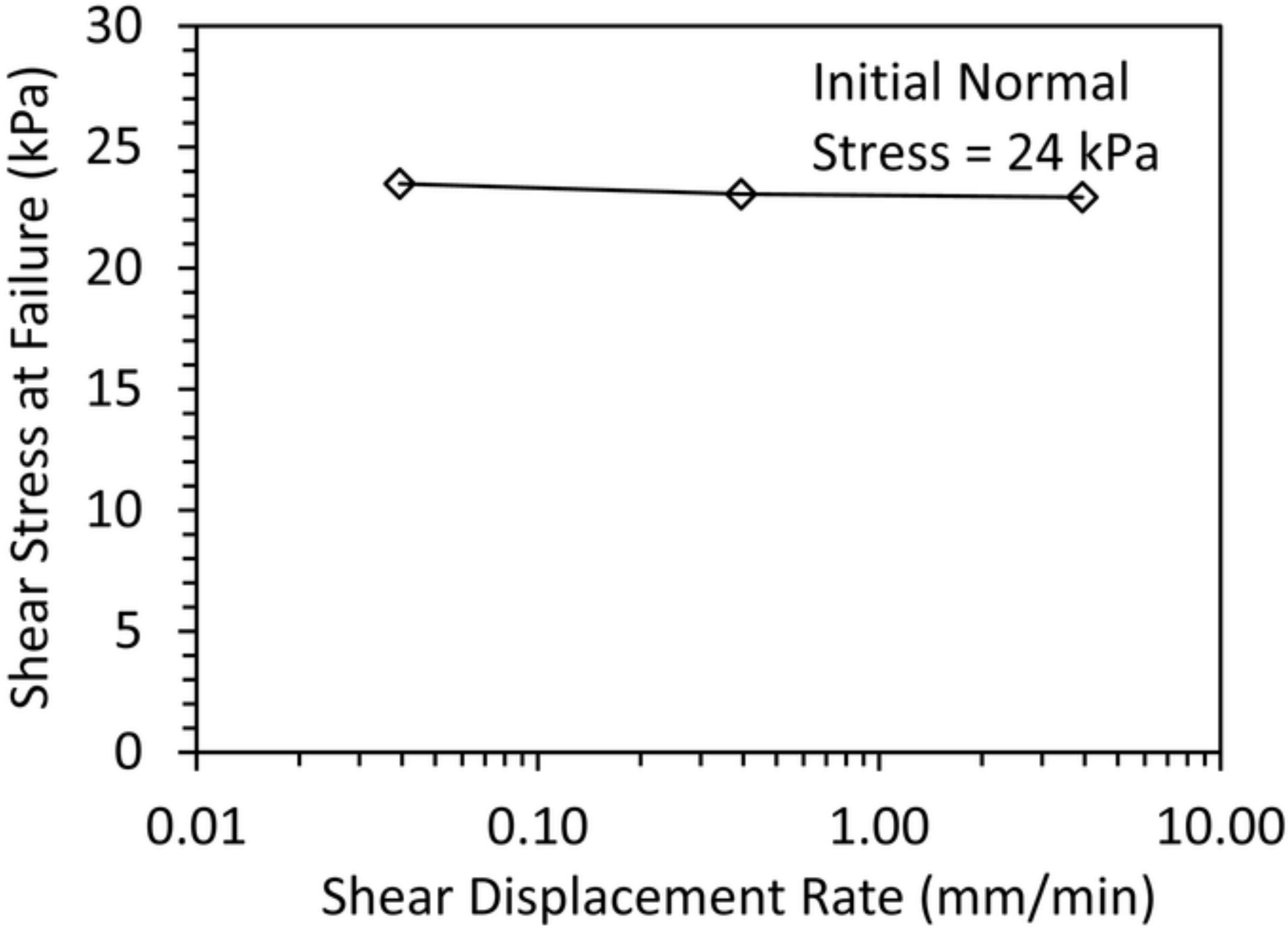
Initial Normal
Stress = 24 kPa
Shear Stress at Failure (kPa)
30
25
20
15
10
5
0
0.01
0.10
1.00
10.00
Shear Displacement Rate (mm/min)

Figure 8

Click here to download Figure Figure 08.tif

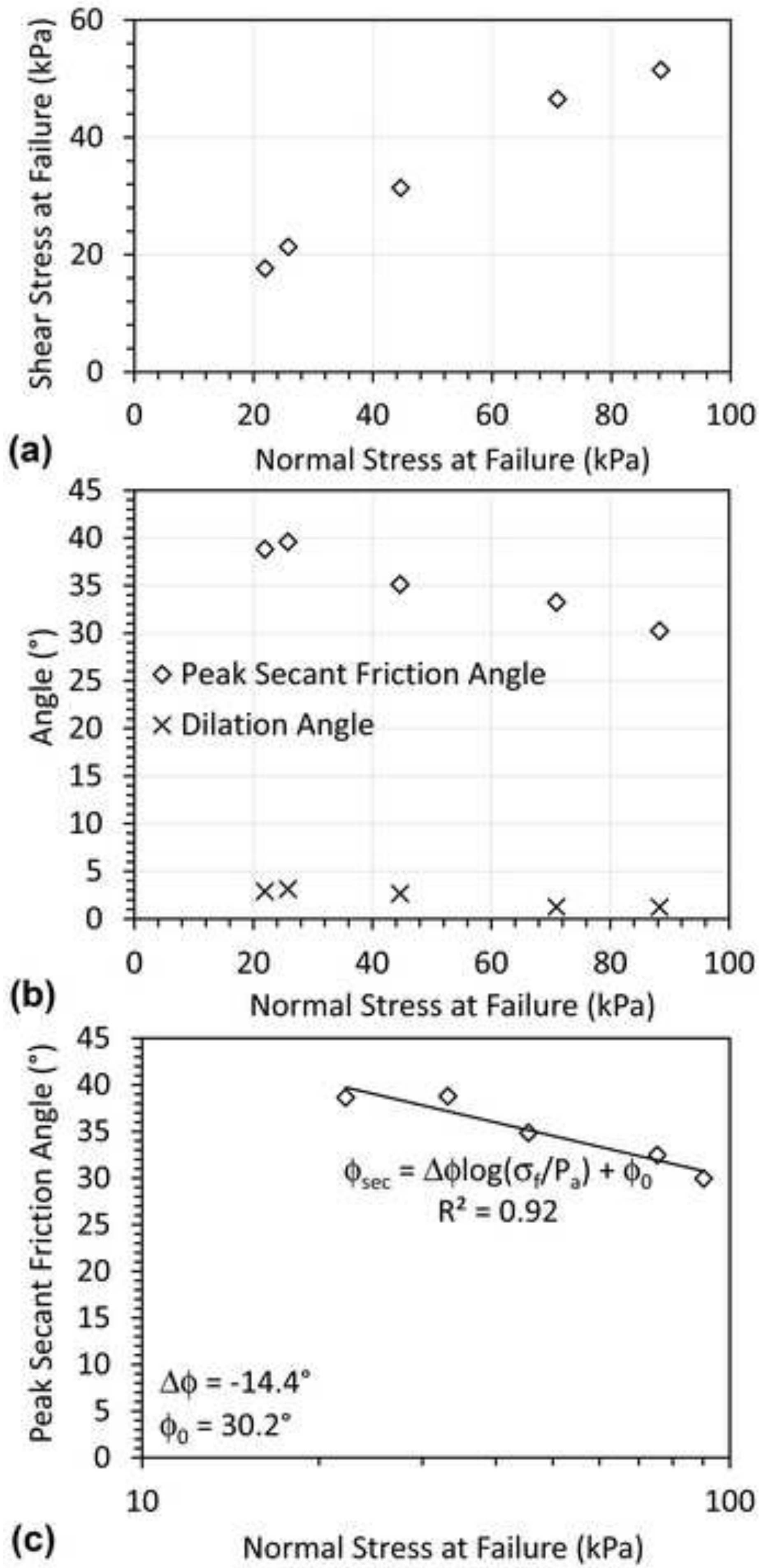

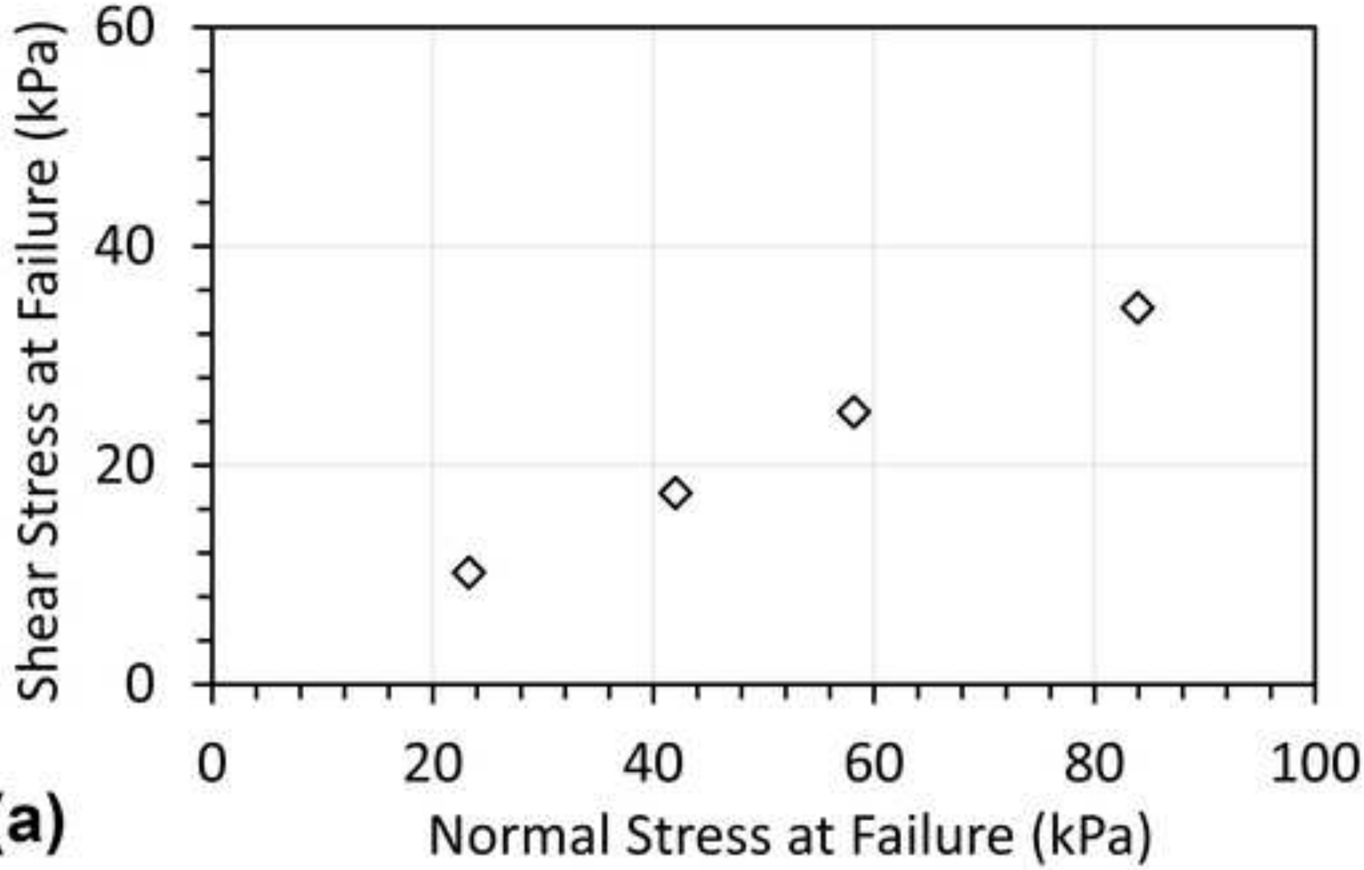

Shear Stress at Failure (kPa)
60
40
20
0
0
20
40
60
80
100
Normal Stress at Failure (kPa)

(a)

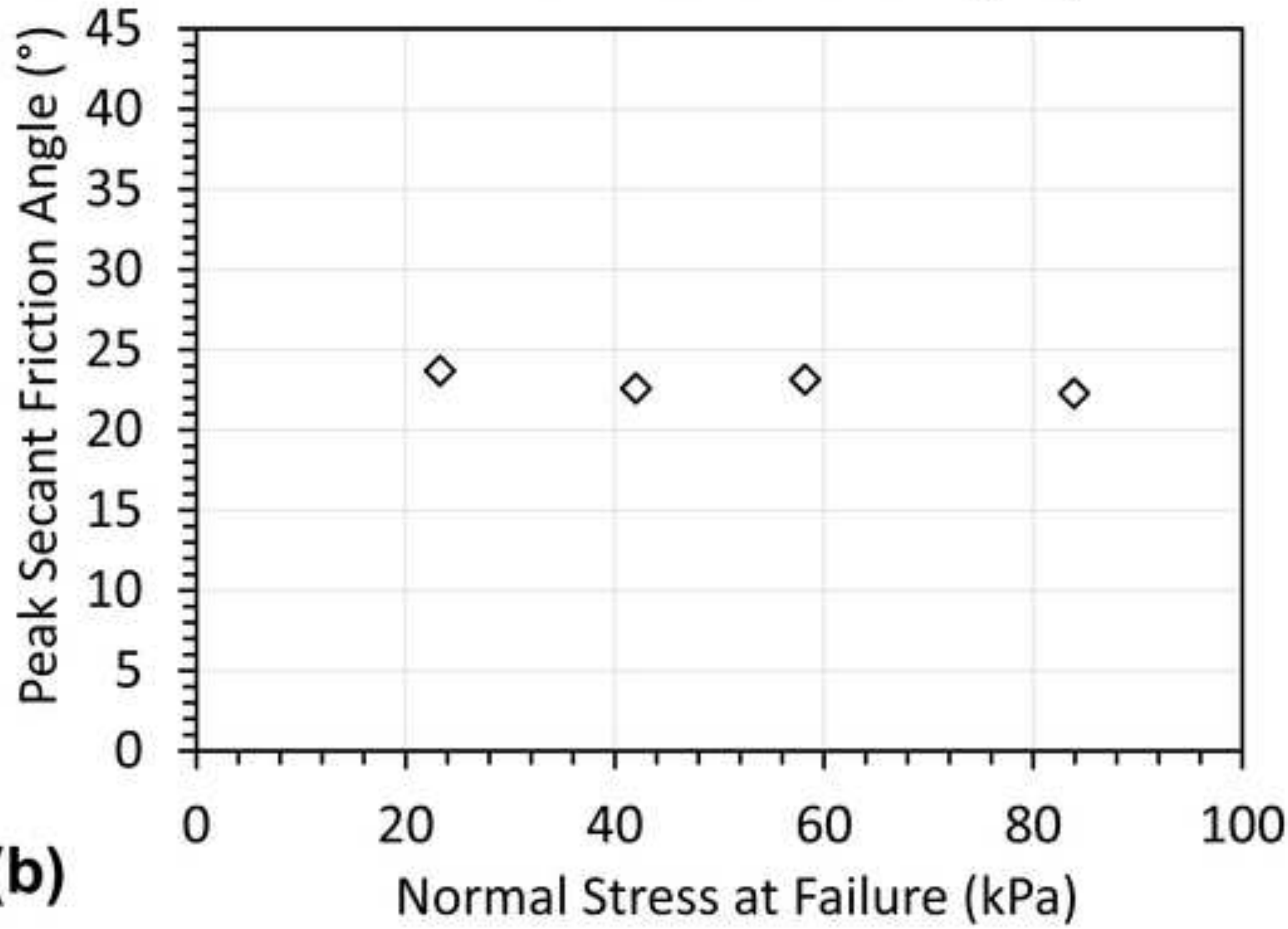

Peak Secant Friction Angle (°)
45
40
35
30
25
20
15
10
5
0
0
20
40
60
80
100
Normal Stress at Failure (kPa)

(b)

Figure 10

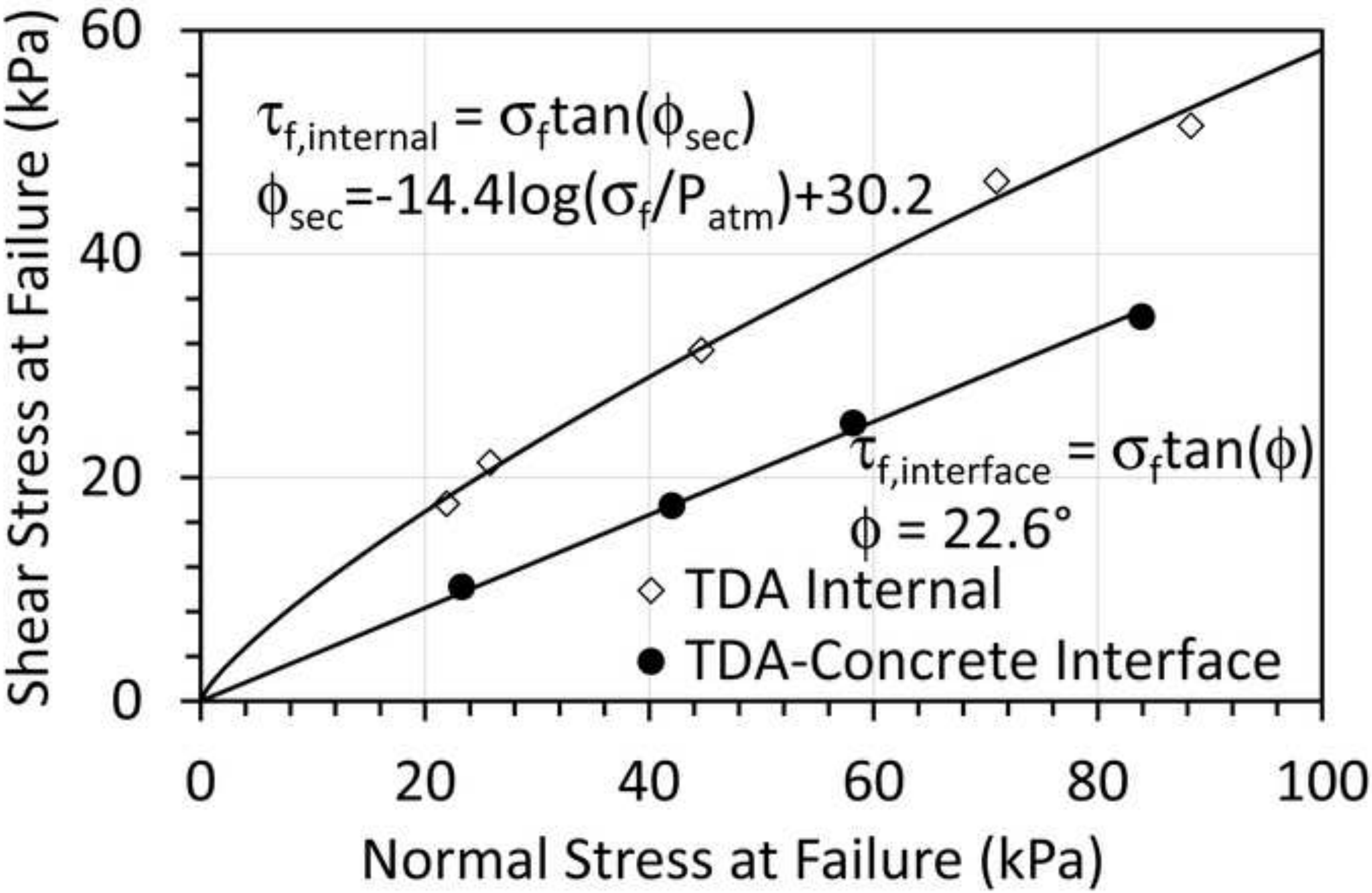

τf,internal = σf tan(φsec)
φsec=-14.4log(σf/Patm)+30.2
τf,interface = σf tan(φ)
φ = 22.6°
TDA Internal
TDA-Concrete Interface
Shear Stress at Failure (kPa)
Normal Stress at Failure (kPa)
0
20
40
60
80
100

Figure 11

Click here to download Figure Figure 11.tif

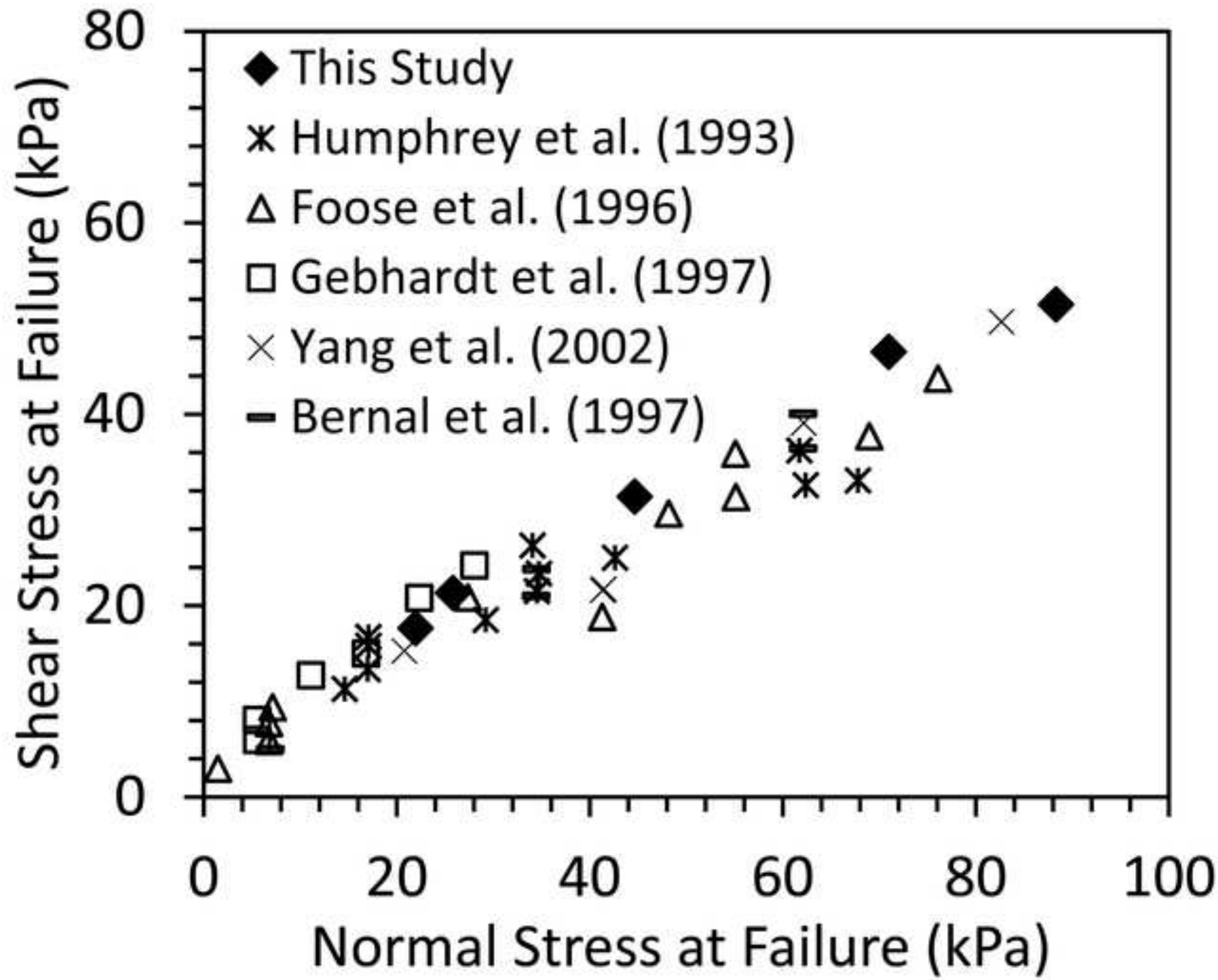

Figure 12

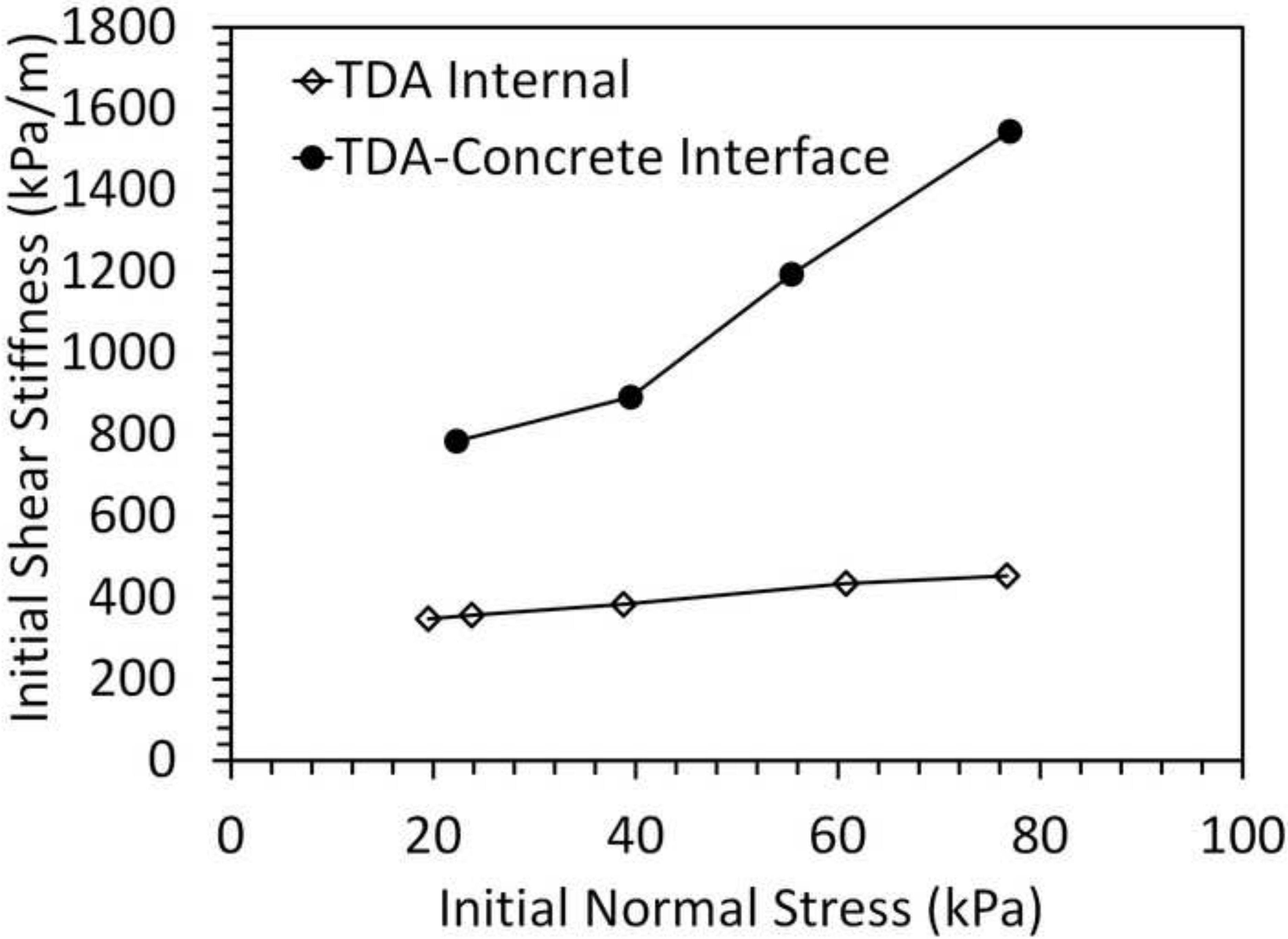

TDA Internal
TDA-Concrete Interface
Initial Shear Stiffness (kPa/m)
0
200
400
600
800
1000
1200
1400
1600
1800
0
20
40
60
80
100
Initial Normal Stress (kPa)